Engineering Solid Mechanics 10 (2022) 325-340

Contents lists available at GrowingScience

Engineering Solid Mechanics

homepage: www.GrowingScience.com/esm

Effect of an edge crack on stress concentration around hole surrounded by functionally graded material layer

Vikas Goyat[a*], Suresh Verma[b] and R. K. Garg[b]

[a]*SRM Institute of Science and Technology, Delhi NCR Campus Ghaziabad, Uttar Pradesh, India*
[b]*Deenbandhu Chhotu Ram University of science and Technology, India*

ARTICLEINFO

Article history:
Received 8 January 2022
Accepted 22 June 2022
Available online
22 June 2022

Keywords:
Functionally graded material
Stress intensity factor
Stress concentration factor
Edge crack
Circular hole
XFEM

ABSTRACT

The present work aims to investigate the effect of an edge crack on the stress concentration around the circular hole surrounded by Functionally Graded Material (FGM) in an infinite plate subjected to uniaxial tensile load. The numerical investigation has been carried out using Extended Finite Element Method (XFEM). Two cases have been analysed in this work, i.e. the whole plate made up of radial FGM and homogeneous material plate having radial FGM layer around the hole. Young's modulus of FGM varies according to exponential and power law function. The relations of stress intensity factor (SIF) and stress concentration factor (SCF) with normalised crack length, Young's modulus ratio, FGM layer thickness and power law index have been presented. It has been observed that the FGM layer case has low SCF around hole than FGM plate case in presence of an edge crack.

1. Introduction

Materials play a key role in the advancement of modern engineering applications and composite materials are commonly used materials for such applications. In the mid of 1980s, a new branch of composite material was discovered by a group of Japanese scientists known as Functionally Graded Materials (FGMs) (Koizumi and Niino, 1995). FGMs have varying composition of its constituents along spatial dimension(s) which provides the smooth variation in material properties along that spatial dimension(s). This smooth variation in material properties eliminates the interfacial problems and makes FGM as a potential material for numerous modern engineering applications where the conventional composite materials fail to perform.

Stress concentration in homogeneous materials is independent of material properties, but in FGM it is significantly affected by the varying material properties. The first brief SCF analysis in FGM structure was traced in the work of Kim and Paulino (2002). A problem of stress concentration in two dimensional FGM plate with circular hole and a pair of shoulder fillets was solved and it was found that by tailoring the FGM one can significantly reduce SCF. The isoparametric graded finite elements were also presented to model the FGM properties within the finite elements. Kubair and Bhanu-chander (2008) provided a detail numerical investigation on an infinite exponential/power law FGM plate for SCF using finite element method (FEM). It was reported that by increasing Young's modulus away from the hole boundary, reduced the SCF and FGM affected the magnitude of stresses but the position of maximum stresses does not change. Yang et al., (2010) analysed the SCF in an infinite FGM plate with circular hole using complex variable theory. Mohammadi et al., (2011) analytically investigated the stiffness and SCF in exponential FGM plate having central circular hole. Yang et al., (2012) reported the effect of varying Young's modulus, plate size and hole eccentricity on SCF in finite FGM plate using complex variable theory. Ashrafi et al., (2013) presented graded boundary elements for three-dimensional elastic field of exponential FGM plate to analyse SCF in the vicinity of circular hole. Sburlati (2013) analytically investigated the reduction in SCF by applying homogeneous/FGM

* Corresponding author.
E-mail addresses: vikasgor@srmist.edu.in (V. Goyat)

doi: 10.5267/j.esm.2022.6.005

layer around the circular hole. Enab (2014) numerically analysed the x-direction, y-direction, radial direction, angular direction graded FGM plate for stress concentration due to an elliptical hole using FEM based analysis software ANSYS. Sburlati et al., (2014) presented analytical as well as FEM analysis of SCF around the circular hole reinforced by power law FGM layer. Shi (2015) analytically studied the elastic stress field of exponential FGM plate having elastic inclusion of circular shape. Gouasmi et al., (2015) presented the FEM analysis of SCF reduction for circular notch in FGM plate as well as in homogeneous plate having FGM layer around the notch using ABAQUS software. Dave and Sharma (2016) studied the moments and stresses in power law FGM plate with circular/elliptical hole using complex variable theory. Yang and Gao (2016) reported the SCF reduction by applying the power law function based FGM layer around an elliptical hole using complex variable theory. Goyat et al., (2017) investigated the SCF reduction around the rounded rectangular hole by the application of power law Titanium-Titanium mono Boride FGM using extended finite element method (XFEM). Yang et al., (2018) evaluated stress field around the arbitrary shape inclusion coated with FGM using the complex variable theory. Goyat et al., (2018a) analysed the SCF for the pair of circular holes in homogeneous panel having reinforced FGM layer around the holes using XFEM. Goyat et al., (2018b) reported the effect of different radial FGM materials on SCF using XFEM.

The Stress Intensity Factor (SIF) is the measure of fracture toughness of cracked structure. This factor was introduced by Irwin (1957) in his well-known work of fracture mechanics. For cracked structure, the stress-based failure analysis, i.e. SCF, cannot be used as the cracked structure has an infinite value of SCF near the crack tip even at low or no load condition (Inglis 1913). Therefore, energy-based Griffith's energy release rate (Griffith 1921) or Irwin's SIF (Irwin 1957) are commonly used for analysis of cracked structure. SIF is a function of crack geometry, structure geometry and load conditions. In FGM, SIF is also a function of variation in material properties. Erdogan and Wu (1997) analysed surface crack problem in an exponential FGM plate under different load conditions. Gu and Asaro (1997) analytically investigated the crack in isotropic and orthotropic FGM plate. Gu et al., (1999) presented a simple approach to calculate SIF in non-homogeneous FGM using FEM. The path independent property of conventional J- integral was found invalid in the FGM though, one can find accurate results by considerably refining the mesh near crack tip along with a very narrow J-domain. Anlas et al. (2000) and Chen et al., (2000) independently presented the modified J-integral formulation for FGM structure, but their work was limited to mode-I fracture problems only. Dolbow and Gosz (2002) proposed a path independent mix mode interaction integral scheme for FGM plate. In this scheme, the auxiliary stresses and displacement field near the crack tip were used same as of homogeneous material and auxiliary strain field was obtained from the auxiliary stress field by using the constitutive relation of FGM. By doing so a new term appears in the formulation to compensate the incompatibility of equations when compared with the work of Anlas et al., (2000). Rao and Rahman (2003) presented a new path independent interaction integral approach, i.e. constant-constitutive tensor approach for SIFs of mix mode fracture problems. The displacement and auxiliary strain field around the crack tip were assumed same as of homogeneous material case and stress field was obtained using constitutive relation with constant constitutive matrix of material properties at the crack tip. Paulino and Kim (2004) gave another approach of path independent interaction integral for mixed mode SIFs in FGM structure. In this formulation, the displacement and strain field were used same as of homogeneous material, but stress field was obtained by constitutive relation of FGM. This formulation violated the equilibrium condition of the relations, therefore, it was known as non-equilibrium formulation. Kim and Paulino (2005) reviewed the different formulations of interaction integral. Singh et al., (2011) numerically investigated the cracks, holes and inclusions in a plane strain FGM plate under mechanical load using XFEM and constant constitutive tensor formulation. Hossei et al., (2013) numerically analysed the crack propagation in FGM plate under thermo-mechanical load condition using XFEM along with non-equilibrium interaction integral formulation.

The literature work discussed here is associated either, reduction of SCF or reduction/analysis of SIF(s) in FGM structures. The effect of SCF reduction, due to the application of FGM, on fracture properties is not found in the literature and this is important in aspect of failure of mechanical structures. In this work, the analysis of SCF and SIF in an infinite plate (FGM plate/ homogeneous plate with FGM layer around the hole) having a central circular hole and an edge crack subjected to uniaxial tensile load is discussed. This work may provide an insight to researchers/designers for SCF reduction around the circular hole without/least affecting the fracture properties.

2. Extended Finite Element Method (XFEM)

The XFEM came into the picture from the work of Belytschko and Black (1999) and Moes et al., (1999). They presented a FEM technique to model the crack growth without re-meshing by using partition of unity approach based discontinuous enrichment functions those were derived from the exact solution of displacement field. These enrichment functions handle the mechanics of crack tip and require additional degree of freedoms to the related nodes. This technique has a high degree of accuracy with comparatively coarse mesh. The XFEM method has widely been used in recent years for investigating the cracking behaviour and fracture trajectory of different cracked components and materials (e.g. Afshar et al., 2015; Ham and Hong 2018; Ameri et al., 2021; Asferg et al., 2007; Golewski et al., 2012; Bergara et al., 2017; Agathos et al., 2018; Aliha et al., 2021, 2022; Mirmohammad et al., 2018; Zeleke et al., 2021; Arora et al., 2018; Agwai et al., 2011; Heidari-Rarani and Sayedain 2019).

Governing Equation

Consider a two-dimensional linear elastostatic domain $\Omega \subset \Re^2$ ($\Re^2$: 2D Euclidian domain) has a set of boundaries Γ as depicted in Fig. 1. Set Γ contains traction free crack surface Γ_c, prescribed displacement boundary Γ_u, traction free hole boundary Γ_h and traction boundary Γ_t.

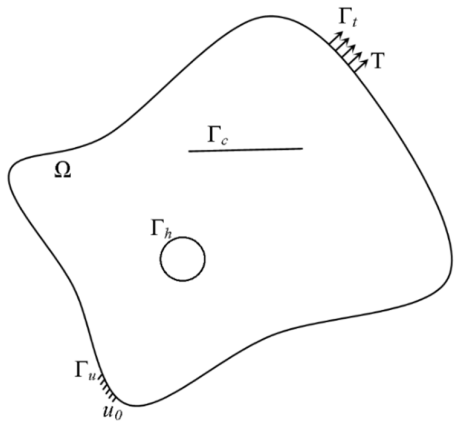

Fig. 1. A linear elastostatic 2D domain having hole and crack subjected to traction (T) and prescribed displacement (u_0).

The equilibrium equation of an elastostatic domain Ω can be stated in terms of body force vector (b), stress tensor (σ) and gradient operator (∇) as (Moes et al., 1999):

$$\nabla \sigma + b = 0 \tag{1}$$

The boundary conditions of Eq. 1 may be expressed as:

$$\sigma \cdot \hat{n} = 0 \quad \text{on } \Gamma_c$$
$$u = u_0 \quad \text{on } \Gamma_u$$
$$\sigma \cdot \hat{n} = 0 \quad \text{on } \Gamma_h$$
$$\sigma \cdot \hat{n} = T \quad \text{on } \Gamma_t$$

where, u is displacement field vector, T is traction, $\hat{n}$ is unit normal vector in outward direction to the domain Ω and u_0 is prescribed displacement. The stress tensor may be written as:

$$\sigma = D(x) : \varepsilon \tag{2}$$
$$\varepsilon = \nabla_s u \tag{3}$$

where, ∇_s, ε and *D(x)* are symmetric gradient operator, strain tensor and constitutive matrix respectively. The constitutive matrix *D(x)* for FGM can be expressed in terms of Young's modulus ($E(x)$) and Poisson's ratio ($\nu(x)$) as:

For plane stress:

$$D(x) = \frac{E(x)}{1-\nu^2(x)} \begin{bmatrix} 1 & \nu(x) & 0 \\ \nu(x) & 1 & 0 \\ 0 & 0 & \dfrac{1-\nu(x)}{2} \end{bmatrix} \tag{4}$$

For plane strain:

$$D(x)=\frac{E(x)}{(1+\nu(x))(1-2\nu(x))}\begin{bmatrix}1-\nu(x) & \nu(x) & 0\\ \nu(x) & 1-\nu(x) & 0\\ 0 & 0 & \frac{1-2\nu(x)}{2}\end{bmatrix} \tag{5}$$

To model the continuous varying Young's modulus ($E(x)$) and Poisson's ratio ($\nu(x)$) within the finite element space isoparametric graded finite elements (Kim & Paulino, 2002) are used in this work. This scheme utilizes nodal shape function (N_i) to determine Young's modulus and Poisson's ratio within the finite element as:

$$E(x) = \sum_{i=1}^{m} N_i E_i \tag{6}$$

$$\nu(x) = \sum_{i=1}^{m} N_i \nu_i \tag{7}$$

Moes et al., (1999) described the weak form of Eq.1 in terms of test function (v^h) and trial displacement function (u^h) as:

$$\int_{\Omega} \sigma(u^h) : \varepsilon(v^h) d\Omega = \int_{\Omega} b \cdot v^h d\Omega + \int_{\Gamma_t} T \cdot v^h d\Gamma \tag{8}$$

To model the holes in XFEM following test and trial function are used.

$$u^h = \sum N_i u_i V(x) \tag{9}$$

where, N_i, u_i and $V(x)$ are nodal shape function, nodal displacement and nodal enrichment function of the finite element respectively. The basic idea of hole enrichment function $V(x)$ is to define the hole boundary within the finite element space. The value of this function is one for the domain body and zero inside the hole i.e.:

$$V(x)=\begin{cases}1 & \text{Outside hole}\,(x \in \Omega)\\ 0 & \text{Inside the hole}\,(x \notin \Omega)\end{cases} \tag{10}$$

In this work, the hole enrichment function is only employed in the vicinity of hole as shown in **Fig. 2.** To further enhance the computational efficiency and to reduce the computational time, the integrals of those nodes which fall inside the hole boundary are simply omitted and set to zero.

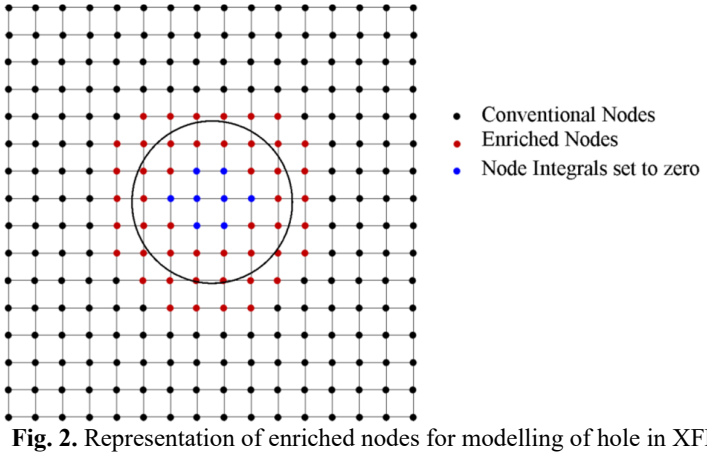

Fig. 2. Representation of enriched nodes for modelling of hole in XFEM

Modelling of Cracks with XFEM: The test and trial function to model the crack is given by Moes et al., (1999).

$$u^h = \sum_{i=I} N_i u_i + \sum_{i=HE} N_i a_i H_s(x) + \sum_{i=CT} N_i \left(\sum_{l=1}^{4} b_i^l F^l(x) \right) \tag{11}$$

The first term of the Eq. 11 is well known classical FEM term of displacement field in finite element space. The second term is heaviside enrichment term which enables the finite element space to handle the crack faces inside the finite element. The third term is crack tip enrichment term to model the displacement behaviour of crack tip. In the Eq.11, u_i is the classical FEM nodal displacement or in another word, it is classical degree of freedom, a_i represents the additional heaviside degree of freedom, $H_s(x)$ is the heaviside enrichment function, b_i^l is the additional degree of freedoms for crack tip, N_i is the finite element shape function, and $F^l(x)$ is the crack tip enrichment function.

Heaviside enrichment function is also known as step function or jump function. It applies to those elements which have the crack face in such a way that the crack split the element into two. This split in the element's domain causes jump behaviour in the displacement field and by incorporating heaviside enrichment function jump behaviour can be modelled easily. Heaviside enriched nodes are shown by circle in Fig. 3. The value of $H_s(x)$ is +1 for nodes above the crack face (green circled nodes) and -1 for nodes below the crack face (red circled nodes). To employ heaviside function one additional degree of freedom (a_i) per node per dimension is required.

Element(s) which contain the crack tip are enriched by crack tip enrichment functions. These functions are derived from the exact solution of displacement field. The mathematical representation of these functions in crack tip in polar coordinate system is as follows:

$$\left\{F^l(r,\theta)\right\}_{l=1}^{4} = \left\{\sqrt{r}\cos\left(\theta/2\right),\ \sqrt{r}\sin\left(\theta/2\right),\ \sqrt{r}\sin\left(\theta/2\right)\sin\theta,\ \sqrt{r}\cos\left(\theta/2\right)\sin\theta\right\} \tag{12}$$

In Eq. 12, r and θ represents crack tip polar coordinates and the second enrichment function i.e. $\sqrt{r}\sin\left(\theta/2\right)$ is discontinuous around crack tip that provides the desired effect to approximate the displacement field near the crack. Other three functions are continuous around the crack tip and used for improvement in the solution of displacement field. Each crack tip enriched node requires eight extra degrees of freedoms. Further, the crack tip enriched nodes are represented by square in **Fig. 3.**

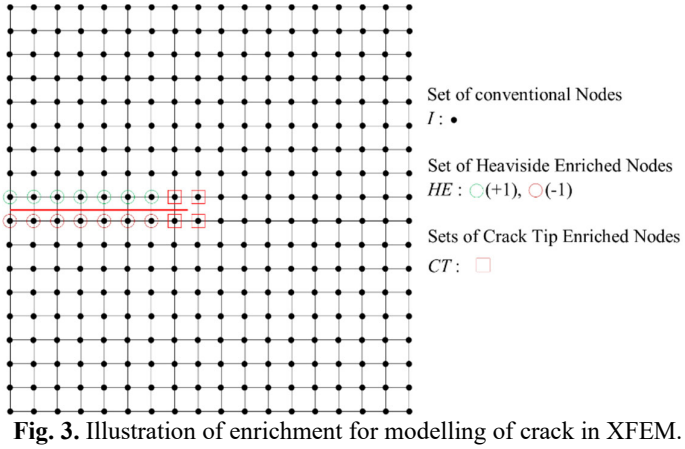

Fig. 3. Illustration of enrichment for modelling of crack in XFEM.

After substituting the trial function u^h of hole (Eq. 9) and crack (Eq. 11) in Eq. 8, one can get the discrete form as:

$$\left[k_{ij}\right]\left\{d_j\right\} = \left\{f_i\right\} \tag{12}$$

where, d is nodal displacement vector, k is stiffness matrix and f represents the nodal force vector. The stiffness matrix can be obtained as:

$$k_{ij}^{\alpha\beta} = \int_{\Omega} \left(B_i^{\alpha}\right)^T D(x) \left(B_j^{\beta}\right) d\Omega \tag{13}$$

$$\alpha = \beta = \{u, a, b\}$$

u : Standard DOF, a : Heaviside DOF, b : Crack Tip DOF

In the matrix form,

$$k_{ij} = \begin{bmatrix} k_{ij}^{uu} & k_{ij}^{ua} & k_{ij}^{ub} \\ k_{ij}^{au} & k_{ij}^{aa} & k_{ij}^{ab} \\ k_{ij}^{bu} & k_{ij}^{ba} & k_{ij}^{bb} \end{bmatrix} \tag{14}$$

In Eq. 13 the B represents basis matrix which can be written as:

$$B_i^u = \begin{bmatrix} (N_i)_{,x} & 0 \\ 0 & (N_i)_{,y} \\ (N_i)_{,y} & (N_i)_{,x} \end{bmatrix} \tag{15}$$

$$B_i^a = \begin{bmatrix} (H_s N_i)_{,x} & 0 \\ 0 & (H_s N_i)_{,y} \\ (H_s N_i)_{,y} & (H_s N_i)_{,x} \end{bmatrix} \tag{16}$$

$$B_i^b = \begin{bmatrix} (F_l N_i)_{,x} & 0 \\ 0 & (F_l N_i)_{,y} \\ (F_l N_i)_{,y} & (F_l N_i)_{,x} \end{bmatrix} \tag{17}$$

The subscript ($_{,x}$) and ($_{,y}$) represents the derivative with respect to x-dimension and y-dimension respectively. Further, the nodal force vector is expressed as:

$$f_i = \left\{ f_i^u \quad f_i^a \quad \left(f_i^b\right)_{l=1}^4 \right\} \tag{18}$$

where,

$$f_i^u = \int_{\Gamma_t} (N_i)^T T d\Gamma_t + \int_{\Omega} (N_i)^T b d\Omega \tag{19}$$

$$f_i^a = \int_{\Gamma_t} (H_s N_i)^T T d\Gamma_t + \int_{\Omega} (H_s N_i)^T b d\Omega \tag{20}$$

$$\left(f_i^b\right)_{l=1}^4 = \int_{\Gamma_t} (F_l N_i)^T T d\Gamma_t + \int_{\Omega} (F_l N_i)^T b d\Omega \tag{21}$$

A different numerical integration scheme is used in XFEM. The enriched elements are subdivided into triangles and then sixth-order triangular Gauss quadrature is applied on crack tip element and forth-order triangular Gauss quadrature is used for heaviside and hole enriched elements. Further, for non-enriched near tip elements the standard forth-order Gauss quadrature and for rest of elements the standard third-order Gauss quadrature is used.

3. Level Set Method

The hole and crack boundaries are traced with the level set method in this work. Level set method was introduced by Osher and Sethian in 1988. This method represents the crack and hole boundaries by a higher dimension function of XFEM mesh. Consider a domain Ω having an arbitrary crack Γ_c as shown in Fig. 4. To model the crack in XFEM, normal and tangential level set functions are required. As the name suggests the normal level set function (ϕ) is evaluated in normal direction of the crack and tangential level set function (ψ) is formed along the tangential direction of the crack.

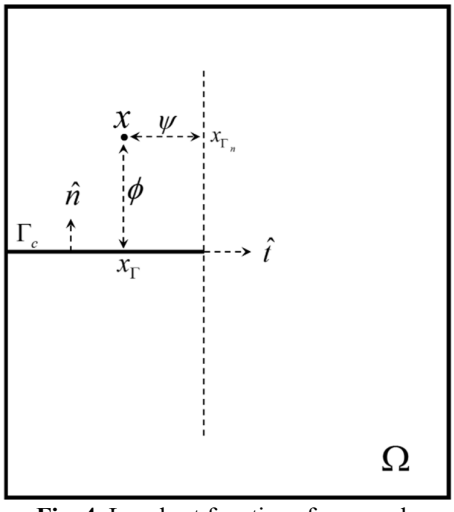

Fig. 4. Level set functions for a crack.

The ϕ is described in such a way that the value of this function found positive above the crack, negative below the crack and zero on the crack. The ψ is calculated in the tangential direction from the normal drawn of the crack tip in such a way that in front of crack tip it is positive and behind the crack tip it is negative. Normal and tangential level set function for an edge crack can be written as:

$$\phi = \left| x - x_\Gamma \right| \cdot \hat{n} \tag{22}$$

$$\psi_1 = \left| x - x_{\Gamma_n} \right| \cdot \hat{t} \tag{23}$$

where, $\hat{n}$, $\hat{t}$, x, x_Γ and x_{Γ_n} are normal direction vector, tangential direction vector, arbitrary point, neariest point on the crack face and nearest point on the normal of crack tip respectively. The elements which require the enrichments can easily be traced by the level set functions. Heaviside enriched elements can be traced by the following conditions:

$$\phi_{\min} * \phi_{\max} \leq 0; \text{ and } \psi_{\max} < 0$$

The crack tip enriched element can be found by the following conditions:

$$\phi_{\min} * \phi_{\max} \leq 0; \text{ and } \psi_{\min} * \psi_{\max} \leq 0$$

The value of heaviside function can also be described by ϕ as:

$$H = sign(\phi); \text{ or } H = \begin{Bmatrix} +1 & if\ \phi \geq 0 \\ -1 & otherwise \end{Bmatrix} \tag{24}$$

Further, one can calculate the crack tip polar coordinates as:

$$r = \sqrt{\phi^2 + \psi^2} \tag{25}$$

$$\theta = \tan^{-1}\left(\frac{\phi}{\psi}\right) \tag{26}$$

For modelling of hole the static level set function ξ is used. It divides the domain Ω into two subdomains in such a way that subdomain Ω_1 represents outside the hole boundary and subdomain Ω_2 represents inside the hole as well as on the hole boundary. By equating the level set function ξ with zero one can trace the hole boundary (Γ_h). For an arbitrary shape hole, the level set function can be written in form of sign distance function as:

$$\xi = \left| x - x_{\Gamma_h} \right| \cdot \hat{n} \tag{27}$$

The ξ for a circular hole can be evaluated easily by using following equation:

$$\xi = \sqrt{(x - x_c)^2 + (y - y_c)^2} - R \tag{28}$$

where, x and y represent an arbitrary point coordinates. The x_c, y_c and R are the coordinates of centre and hole radius respectively.

4 Interaction Integral

To evaluate the SIF, the path independent non-equilibrium interaction integral formulation (Paulino & Kim 2004) is used in this work. This formulation uses the same auxiliary displacement and strain field as of homogeneous materials with Young's modulus and Poisson's ratio of crack tip, but the auxiliary stress field is obtained by using constitutive relation with constitutive matrix of FGM material as:

$$\sigma_{ij}^2 = C_{ijkl}(x)\varepsilon_{kl}^2 \tag{29}$$

It is clear from the Eq. 29 that it does not satisfy the equilibrium condition which is given by:

$$\sigma_{ij}^2 = \left(C_{ijkl}\right)_{tip}\varepsilon_{kl}^2 \tag{30}$$

According to this formulation the interaction integral (M) over a close path Γ ($\Gamma = \Gamma_0 + \Gamma_1 + \Gamma_2 + \Gamma_3$) around the crack tip (as shown in **Fig. 5**) can be expressed as:

$$M = \int_A \left\{ \sigma_{ij}^1 u_{i,1}^2 + \sigma_{ij}^2 u_{i,1}^1 - \frac{1}{2}\left(\sigma_{ij}^1 \varepsilon_{ij}^2 + \sigma_{ij}^2 \varepsilon_{ij}^1\right)\delta_{1j} \right\} q_{,j} dA + \int_A \left\{ \underline{\sigma_{ij,j}^2 u_{i,1}^1} - D_{ijkl,1}\varepsilon_{kl}^1 \varepsilon_{ij}^2 \right\} q dA \tag{31}$$

where

$$\sigma_{ij,j}^2 = \underline{\left(D_{ijkl}\right)_{tip}\varepsilon_{kl,j}^2} + D_{ijkl,j}(x)\varepsilon_{kl}^2 + \left(D_{ijkl}(x) - \left(D_{ijkl}\right)_{tip}\right)\varepsilon_{kl,j}^2 \tag{32}$$

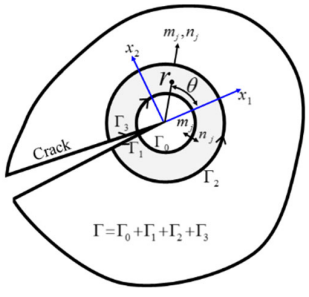

Fig. 5. Illustration of a closed path $\Gamma = \Gamma_0 + \Gamma_1 + \Gamma_2 + \Gamma_3$ for interaction integral in a cracked domain.

The superscript (1 and 2) denotes the actual and auxiliary fields respectively. The subscript ($,_1$) represents the derivative with dimension x_1. The q represents plateau-type weight function varying from Γ_0 to Γ_2 as $q = 1$ at Γ_0 and $q = 0$ at Γ_2. The underline terms of Eq. 31 appeared to compensate the non-equilibrium condition and underline term of Eq. 32 vanishes. To obtain the SIFs the Eq. 31 is compared with the following standard equation.

$$M = \frac{2}{E'}\left[\left(K_I^1\right)\left(K_I^2\right)+\left(K_{II}^1\right)\left(K_{II}^2\right)\right] \tag{33}$$

The SIF of mode-I is evaluated by putting $K_I^2 = 1$ and $K_{II}^2 = 0$

$$M = \frac{2}{E'_{tip}} K_I^1 \quad (\text{By using } K_I^2 = 1,\ K_{II}^2 = 0) \tag{34}$$

Similar for mode-II

$$M = \frac{2}{E'_{tip}} K_{II}^1 \quad (\text{By using } K_I^2 = 0,\ K_{II}^2 = 1) \tag{35}$$

where, $E'_{tip} = E_{tip}/(1-v_{tip}^2)$ for plane strain and $E'_{tip} = E_{tip}$ for plane stress.

5. Results and Analysis

A XFEM based MATLAB computer code has been developed to solve the problem of SCF and SIF in an infinite plate subjected to uniaxial tensile load. Eight node isoparametric graded quadrilateral elements are used to model the nonhomogeneous behaviour of FGM. Two thin square plates of dimension 20 times to the diameter of the hole are assumed with a central circular hole and an edge crack. First plate is made up of radial FGM and second consist FGM layer around the circular hole as illustrated in **Figs.** 6(a) and 6(b) respectively. Young's modulus of FGM varies according to exponential and power law function along the radial direction of hole, whereas the Poisson's ratio is kept constant (Yang et al., 2010).

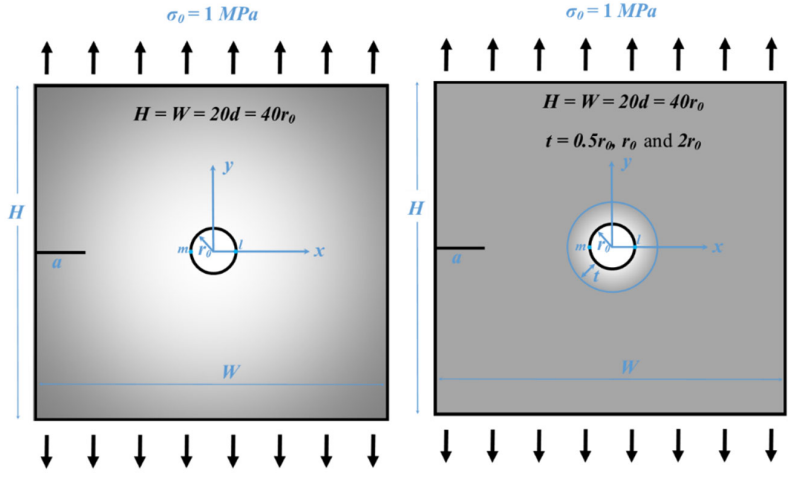

(a) (b)

Fig. 6. (a) FGM plate with hole and edge crack (b) homogeneous plate having edge crack and hole reinforced with FGM layer subjected to uniaxial tensile far-field stress.

Exponential function

$E(r) = E_1 e^{\left(\left(\frac{1}{R^*}\ln E^*\right)r^*\right)}$; for FGM plate

$E(r) = E_1 e^{\left(\left(\frac{1}{t}\ln E^*\right)r^*\right)}$; for FGM layer

$v(r) = v = 0.3$

Power law function

$$E(r) = E_1\left[1+\left(E^*-1\right)\left(\frac{r^*}{R^*}\right)^n\right]; \text{ for FGM plate}$$

$$E(r) = E_1\left[1+\left(E^*-1\right)\left(\frac{r^*}{t}\right)^n\right]; \text{ for FGM layer}$$

$$\nu(r)=\nu=0.3$$

where, $E^*=\frac{E_2}{E_1}$, $r^*=r-r_0$, $R^*=R-r_0$ and $R=\sqrt{\left(\frac{W}{2}\right)^2+\left(\frac{H}{2}\right)^2}$

The r, r_0, E_1, E_2, E^*, ν, n and t represent radial coordinate, hole radius, Young's modulus of material-I, Young's modulus of material-II, Young's modulus ratio, Poisson's ratio, power law index and FGM layer thickness respectively.

5.1 Validation of computer code

The reliability and accuracy of developed computer code have been tested with published literature. For this purpose, the computer code is tuned to solve the problems of Yang et al., (2010) – FGM plate with hole subjected to uniaxial tensile load, Sburlati et al., (2014) – homogeneous plate having circular hole reinforced with FGM layer subjected to uniaxial tensile load and Gross and Srawley (1964) – homogeneous plate with edge crack under tensile load shown in **Figs. 7(a), 7(c) and 7(e)** respectively.

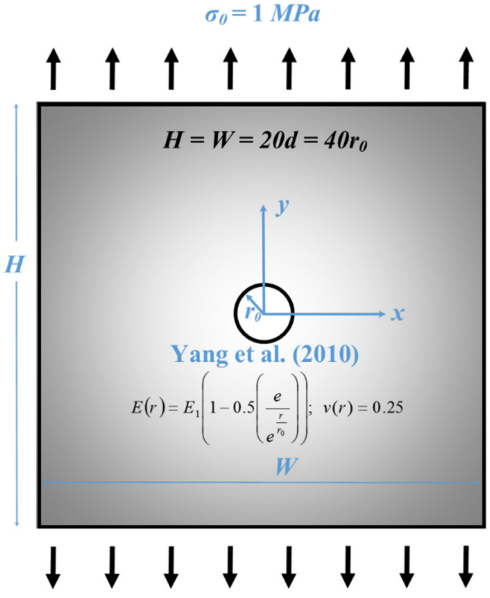

(a)

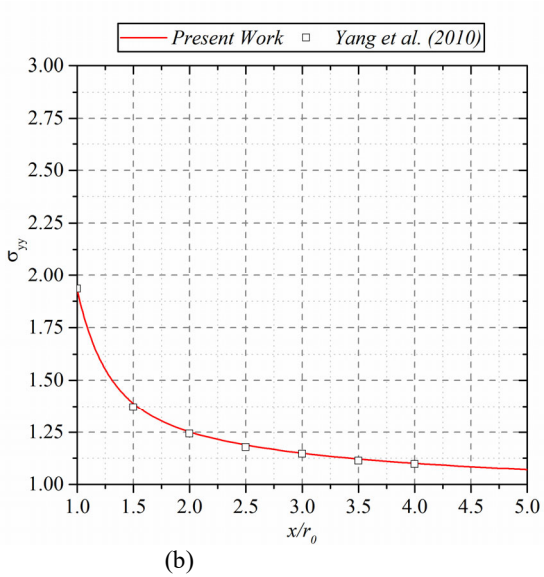

(b)

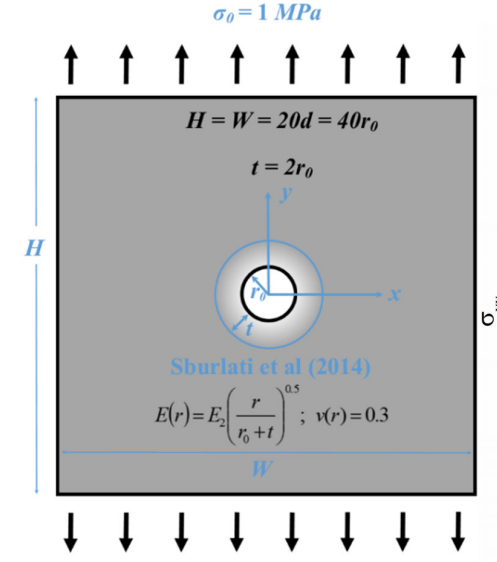

(c)

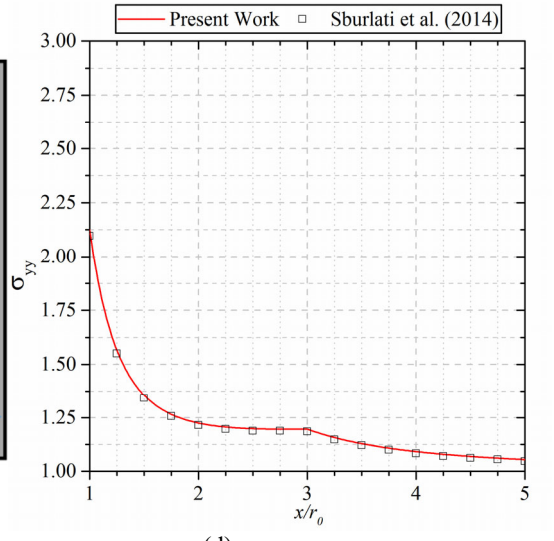

(d)

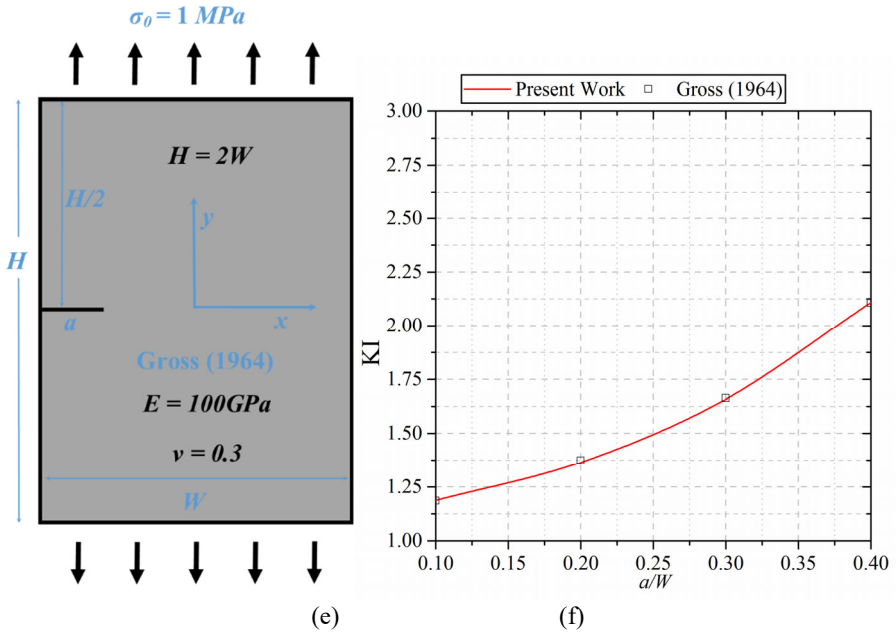

Fig. 7. Problem configuration and obtained results for validation (a) FGM plate with circular hole subjected to uniaxial tensile load (b) stress distribution along x-axis around circular hole in FGM plate (c) homogeneous material plate having circular hole reinforced with FGM layer subjected to tensile load (d) variation of normal stress x-axis due to FGM layer (e) homogeneous material plate with edge crack subjected to tensile far field stress (f) variation of SIF with normalised crack length.

The obtained results of validation problems, i.e. stress distribution along normalised x-axis in FGM plate, variation of normal stress with normalised x-axis due hole reinforced with FGM layer and variation of SIF with normalised crack length are reported in **Figs. 7(b), 7(d) and 7(f)** respectively, along with the results of published references. A good agreement is found between the results obtained from developed computer code and the results reported in the literature and a maximum error of < 2% is noticed.

5.2 FGM plate with hole and edge crack

The effect of FGM functions, Young's modulus ratio (E^*), power law index (n) and normalised crack length (a/W) on SCF and SIF is analysed for FGM plate with circular hole and edge crack subjected to uniaxial tensile load (see Fig. 6(a)). Fig. 8 shows the variation of SIF of mode-I (KI) and SCFs (K_{tR} and K_{tL}) with normalised crack length (a/W) for different values of n in power law FGM plate of E^* = 5. It is observed that KI increases with increase in a/W irrespective of the value of n. For n = 0.2 and 0.5, the value of KI is found higher than homogeneous plate case i.e. n = 0. The value of KI for FGM plates having n = 1, 2 and 5 is observed to be higher than that of homogeneous plate for lower values of a/W but, for higher values of a/W, the KI is found lower than the homogeneous plate.

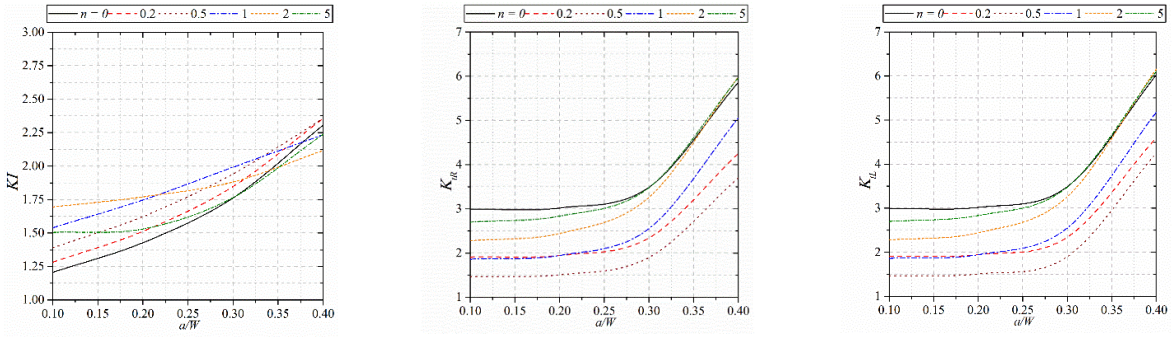

Fig. 8. variation of (a) KI (b) K_{tR} and (c) K_{tL} with normalised crack length (a/W) for different values of power law index (n).

Two SCFs K_{tR} i.e. for right half plate and K_{tL} i.e. for the left half plate, are used in this work. The left half plate consists edge crack and crack properties may affect the stress concentration of left half plate. Therefore, two SCFs are convenient to describe this work. These SCFs are calculated as:

$$K_{tR} = \frac{\sigma_{\max}(\text{Right half plate})}{\sigma_0} \qquad K_{tL} = \frac{\sigma_{\max}(\text{Left half plate})}{\sigma_0}$$

The K_{tR} and K_{tL} are observed constant up to $a/W = 0.2$, beyond that K_{tR} and K_{tL} increase with increase in a/W for all values of n. For $n \leq 1$, it can be stated that the value of K_{tR} and K_{tL} are found lower than homogeneous plate. For $n > 1$, the value of K_{tR} and K_{tL} are noticed to be lower for lower values of a/W and slightly higher for higher values of a/W as compared to homogeneous plate. When comparing the value of K_{tR} with K_{tL}, it is found that the value of K_{tL} is slightly higher than K_{tR} for $a/W \geq 0.3$ and for rest values of a/W, the K_{tR} and K_{tL} are found same. It is also noticed that the $n = 0.5$ shows the least value of SCFs. The effect of Young's modulus ratio (E^*) on KI, K_{tR} and K_{tL} is analysed for power law index $n = 0.5$ and shown in Figs. 9(a), (b) and (c) respectively. It is observed that the KI increases with increase in E^* and a/W. The difference in KI of FGM plate and homogeneous plate is found decreasing with increase in a/W. The SCFs (K_{tR} and K_{tL}) decrease with increase in E^* for a particular value of a/W. The K_{tR} and K_{tL} are noted to be constant for $a/W < 0.2$ and then sharp increase is noticed with further increase in a/W. The K_{tL} has higher value than K_{tR} for $a/W > 0.25$ for all values of E^*.

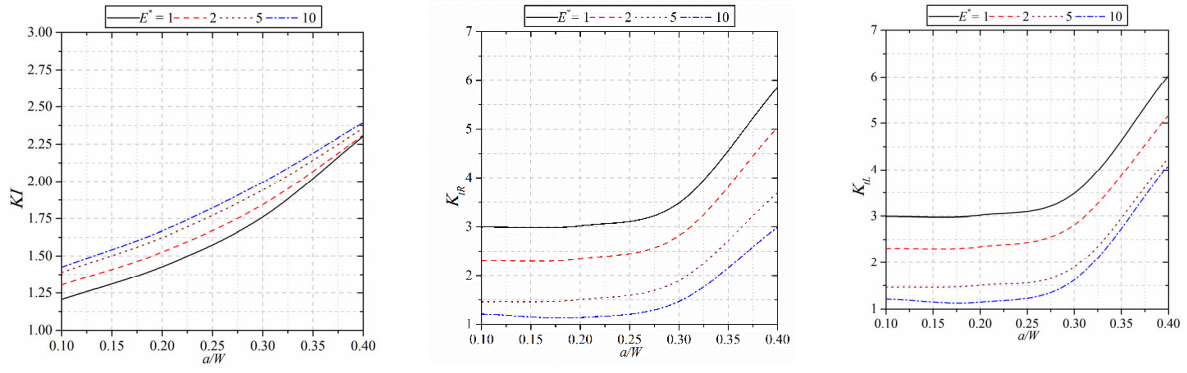

(a) (b) (c)

Fig. 9. effect of Young's modulus ratio on the variation of (a) KI (b) K_{tR} and (c) K_{tL} with normalised crack length (a/W) for power law index ($n = 0.5$).

For radial exponential FGM plate, the effect of Young's modulus ratio (E^*) on KI, K_{tR} and K_{tL} is shown in the **Figs.** 10(a), (b) and (c) respectively. The KI increases with increase in a/W for all values of E^*. The difference in the value of KI of FGM plate and homogeneous plate ($E^* = 1$) decreases with increase in a/W further, this difference is positive for $a/W \leq 0.35$ and negative for $a/W > 0.35$. The trend of K_{tR} and K_{tL} are found similar to the case of power law FGM with $n = 0.5$ but, the amount of reduction in the value of SCFs is found less in exponential FGM case.

5.3 Homogeneous plate with edge crack and hole reinforced with FGM layer

In this section, the effect of different FGM layers (power law and exponential) and their properties such as power law index, FGM layer thickness and Young's modulus ratio is analysed on KI, K_{tR} and K_{tL} for a homogeneous plate with edge crack and circular hole reinforced by a FGM layer under to uniaxial tensile far-field stress (see **Fig. 6(b)**).

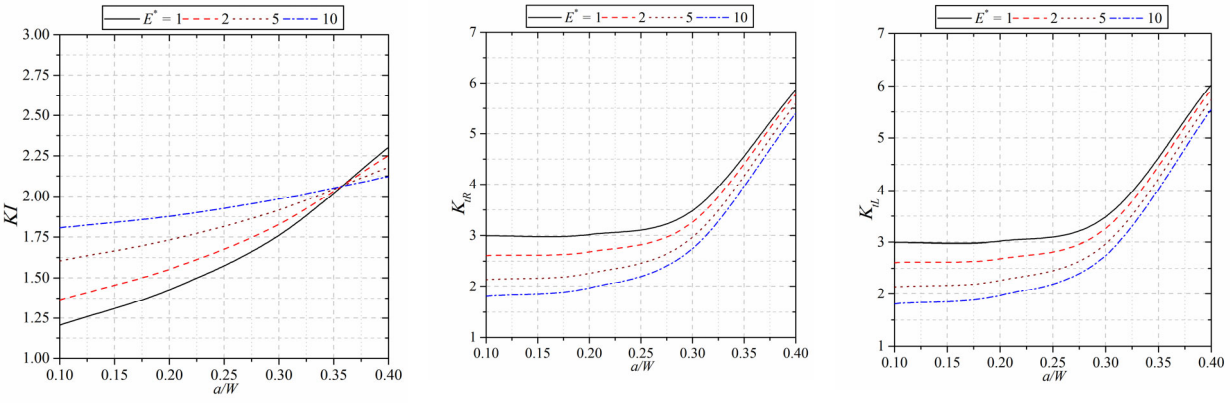

(a) (b) (c)

Fig. 10. effect of Young's modulus ratio on the variation of (a) KI (b) K_{tR} and (c) K_{tL} with normalised crack length (a/W) for exponential FGM

Fig. 11(a) shows the relation of *KI* with *a/W* for different values of *n*, while E^* and FGM layer thickness (*t*) are taken as 5 and r_0 respectively. It is noticed that the *KI* increases with increase in *a/W* and *n*. Though, the amount of increase in the value of *KI* with *n* is found insignificant for *a/W* < 0.25.

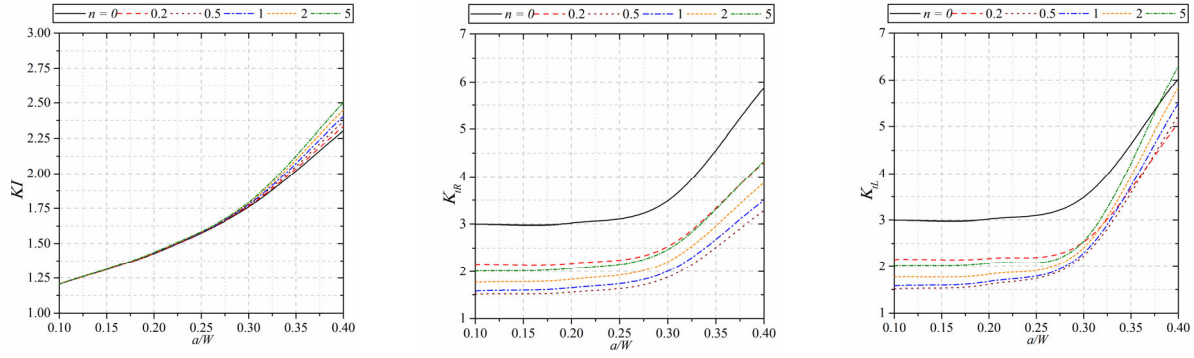

(a) (b) (c)

Fig. 11. effect of power law index (*n*) on the variation of (a) *KI* (b) K_{tR} and (c) K_{tL} with normalised crack length (*a/W*) for power law FGM layer with E^* = 5 and t = r_0.

The variation of SCFs K_{tR} and K_{tL} with *a/W* for different values of *n* are shown in Fig. 11(b) and (c) respectively. It is noted from the figures that the K_{tR} and K_{tL} are first constant and then increase with increase in *a/W*. For a particular value of *a/W*, it can be stated that the K_{tR} and K_{tL} are first decrease and then increase with increase in power law index *n.* Further, it is found that the power law index *n* = 0.5 has least value of K_{tR} and K_{tL} for maximum range of *a/W*.

The effect of E^* on relation of *KI*, K_{tR} and K_{tL} with *a/W* for power law FGM layer with *n* = 0.5 and layer thickness t = r_0 is reported in Figs. 12(a), (b) and (c) respectively. It is noticed that the *KI* increases with increase in *a/W*. The *KI* of FGM layer cases follows the *KI* of homogeneous plate (E^* = 1) for *a/W* < 0.3 and then increases with increase in E^*. The K_{tR} and K_{tL} are found constant up to *a/W* = 0.2 and then sharply increase with further increase in *a/W*. For a particular value of *a/W*, the K_{tR} decreases with increase in E^* up to E^* = 5 and no further significant decrease is observed for E^* = 10. For *a/W* ≤ 0.3, the K_{tL} decreases with increase in E^* up to E^* = 5 and E^* = 10 has same value as of E^* = 5. Further, for *a/W* > 0.3, it is found that K_{tL} of E^* = 5 and 10 are slightly higher than that of E^* = 2.

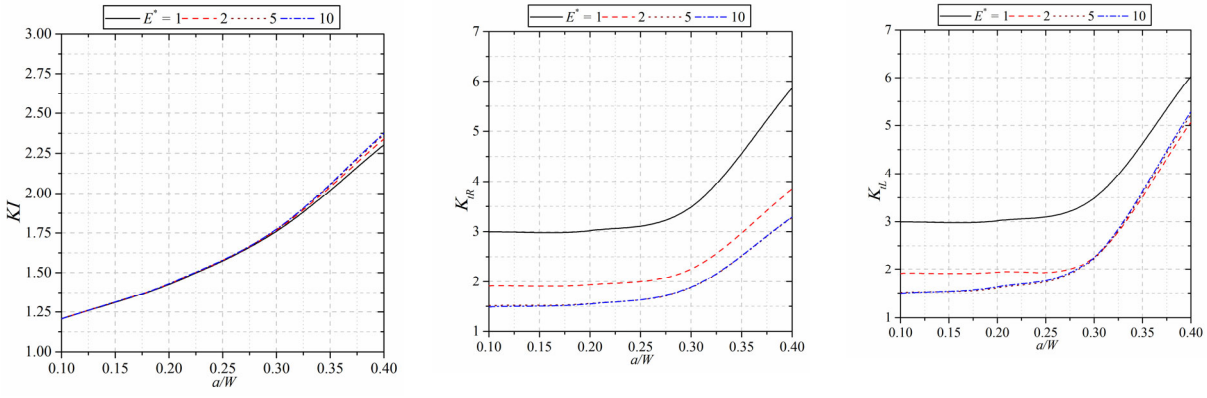

(a) (b) (c)

Fig. 12. effect of Young's modulus ratio (E^*) on the relation of (a) *KI* (b) K_{tR} and (c) K_{tL} with normalised crack length (*a/W*) for power law FGM layer with *n* = 0.5 and t = r_0.

Figs. 13(a), (b) and (c) show the effect of FGM layer thickness (*t*) on variation of *KI*, K_{tR} and K_{tL} with *a/W* respectively. It is noted that the effect of *t* on *KI* is insignificant for *a/W* ≤ 0.25 and for *a/W* > 0.25, the *KI* increases with increase in *t.* The trends of K_{tR} and K_{tL} for FGM layer are found similar as of homogeneous plate, but the values are significantly reduced than the homogeneous plate. The value of K_{tL} is observed higher than K_{tR} for *a/W* > 0.2. Further, it is noticed that value of K_{tR} and K_{tL} decrease with increase in *t*.

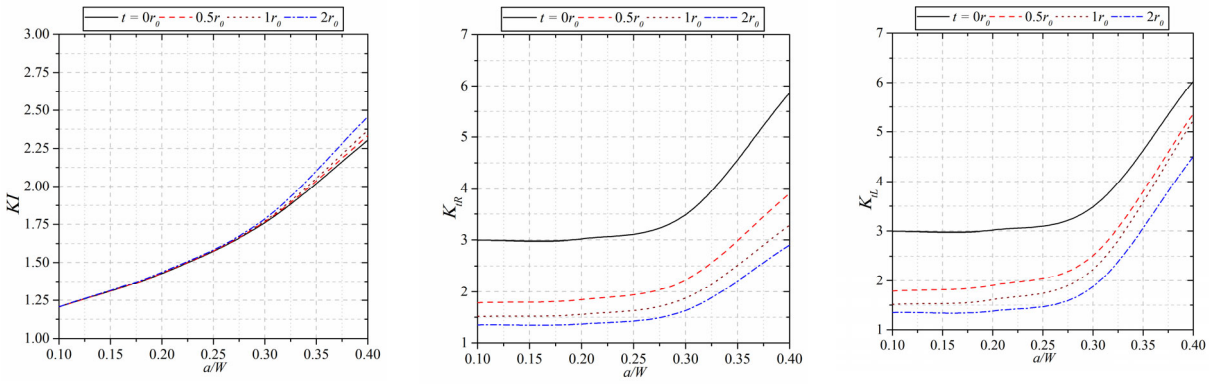

(a) (b) (c)

Fig. 13. effect of FGM layer thickness (t) on the variation of (a) KI (b) K_{tR} and (c) K_{tL} with normalised crack length (a/W) for power law FGM layer with $E^* = 5$ and $n = 0.5$.

The homogeneous plate having circular hole with exponential FGM layer of $t = r_0$ and an edge crack has been analysed for KI, K_{tR} and K_{tL}. **Fig. 14(a)** depicts the relation of KI with a/W for various values of E^*. It is found that the KI increases with increase in E^* and a/W but the increase in KI with E^* is found insignificant for $a/W < 0.3$. **Figs.** 14(b) and (c) show the relation of K_{tR} and K_{tL} with a/W for various values of E^*. The K_{tR} and K_{tL} are noticed to be constant up to $a/W = 0.25$ and increase with further increase in a/W. For a particular value of a/W, the K_{tR} and K_{tL} are first decrease and then increase with increase in E^*.

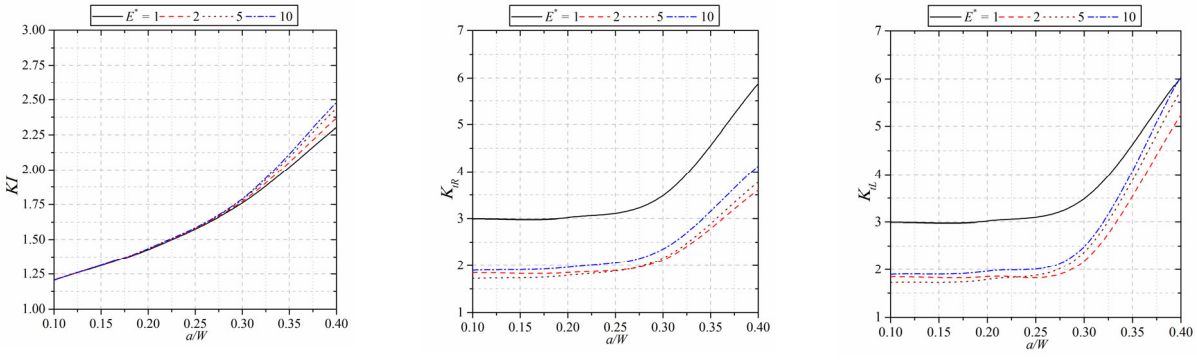

(a) (b) (c)

Fig. 14. effect of Young's modulus ratio (E^*) on the relation of (a) KI (b) K_{tR} and (c) K_{tL} with normalised crack length (a/W) for exponential FGM layer of $t = r_0$.

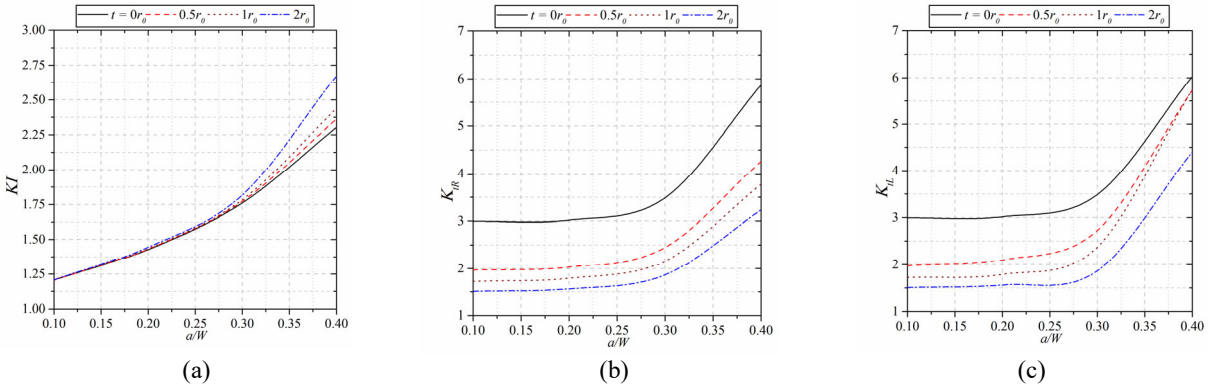

(a) (b) (c)

Fig. 15. effect of FGM layer thickness (t) on the variation of (a) KI (b) K_{tR} and (c) K_{tL} with normalised crack length (a/W) for exponential FGM layer with $E^* = 5$.

The effect of FGM layer thickness (t) on the variation of KI, K_{tR} and K_{tL} with a/W is shown in the **Figs.** 15(a), (b) and (c) respectively, for exponential FGM layer with $E^* = 5$. The KI increases with increase in a/W for all values of t. The KI value of FGM layer follow KI value of homogeneous plate for $a/W \leq 0.25$, beyond this KI increases with increase in t. The K_{tR} and K_{tL} are observed to be constant up to $a/W = 0.2$ and then increase with further increase in a/W. The value of K_{tR} and K_{tL} decrease with increase in t.

6. Conclusions

The effect of SCF reduction by the application of FGM (power law and exponential) on SIF of crack has been analysed for a plate with a hole and an edge crack subjected to uniaxial tensile load. In this work, two cases have been analysed first the whole plate made up of radial FGM and second homogeneous plate having a radial FGM layer around the hole. In both cases the power law FGM with power law index $n = 0.5$ provides the least value of SCFs. The SIF is significantly affected by the Young's modulus ratio (E_2/E_1) in FGM plate case, but FGM layer has insignificant effect on SIF for smaller crack length. Further, an increase in the thickness of FGM layer significantly reduces the SCF without affecting the SIF much for smaller crack length. Therefore, it is better to use FGM layer instead of FGM plate to reduce SCF in presence of edge crack.

References

Afshar, A., Daneshyar, A., & Mohammadi, S. (2015). XFEM analysis of fiber bridging in mixed-mode crack propagation in composites. *Composite Structures, 125*, 314-327.

Agathos, K., Ventura, G., Chatzi, E., & Bordas, S. P. (2018). Stable 3D XFEM/vector level sets for non-planar 3D crack propagation and comparison of enrichment schemes. *International Journal for Numerical Methods in Engineering, 113*(2), 252-276.

Agwai, A., Guven, I., & Madenci, E. (2011). Predicting crack propagation with peridynamics: a comparative study. *International journal of fracture, 171*(1), 65-78.

Aliha, M. R. M., Ebneabbasi, P., reza Karimi, H., & Nikbakht, E. (2021). A novel test device for the direct measurement of tensile strength of rock using ring shape sample. *International Journal of Rock Mechanics and Mining Sciences, 139*, 104649.

Aliha, M. R. M., Kucheki, H. G., & Berto, F. (2022). Numerical analysis of crack initiation angles and propagation paths in adhesively bonded joints under mixed mode I/II loading using a novel test specimen. *Procedia Structural Integrity, 39*, 393-402.

Ameri, B., Taheri-Behrooz, F., & Aliha, M. R. M. (2021). Evaluation of the geometrical discontinuity effect on mixed-mode I/II fracture load of FDM 3D-printed parts. *Theoretical and Applied Fracture Mechanics, 113*, 102953.

Anlas, G., Santare, M. H., & Lambros, J. (2000). Numerical calculation of stress intensity factors in functionally graded materials. *International Journal of Fracture, 104*(2), 131-143.

Arora, P., Srivastava, S., Lohumi, M., & Kumar, H. (2018). Progressive damage response and crack growth direction for multiple through cracks of laminated composite finite plate. *Engineering Solid Mechanics, 6*(4), 371-389.

Asferg, J. L., Poulsen, P. N., & Nielsen, L. O. (2007). A consistent partly cracked XFEM element for cohesive crack growth. *International Journal for Numerical Methods in Engineering, 72*(4), 464-485.

Ashrafi, H., Asemi, K., & Shariyat, M. (2013). A three-dimensional boundary element stress and bending analysis of transversely/longitudinally graded plates with circular cutouts under biaxial loading. *European Journal of Mechanics-A/Solids, 42,* 344-357.

Belytschko, T., & Black, T. (1999). Elastic crack growth in finite elements with minimal remeshing. *International journal for numerical methods in engineering, 45*(5), 601-620.

Bergara, A., Dorado, J. I., Martin-Meizoso, A., & Martínez-Esnaola, J. M. (2017). Fatigue crack propagation in complex stress fields: Experiments and numerical simulations using the Extended Finite Element Method (XFEM). *International Journal of Fatigue, 103*, 112-121.

Chen, J., Wu, L., & Du, S. (2000). A modified J integral for functionally graded materials. *Mechanics research communications, 27*(3), 301-306.

Dave, J. M., & Sharma, D. S. (2016). Stresses and moments in through-thickness functionally graded plate weakened by circular/elliptical cut-out. *International Journal of Mechanical Sciences, 105*, 146-157.

Dolbow, J. E., & Gosz, M. (2002). On the computation of mixed-mode stress intensity factors in functionally graded materials. *International Journal of Solids and Structures, 39*(9), 2557-2574.

Enab, T. A. (2014). Stress concentration analysis in functionally graded plates with elliptic holes under biaxial loadings. *Ain Shams Engineering Journal, 5*(3), 839-850.

Erdogan, F., & Wu, B. H. (1997). The surface crack problem for a plate with functionally graded properties.

Golewski, G. L., Golewski, P., & Sadowski, T. (2012). Numerical modelling crack propagation under Mode II fracture in plain concretes containing siliceous fly-ash additive using XFEM method. *Computational Materials Science, 62*, 75-78.

Gouasmi, S., Megueni, A., Bouchikhi, A. S., Zouggar, K., & Sahli, A. (2015). On the reduction of stress concentration factor around a notch using a functionally graded layer. *Materials Research, 18*, 971-977.

Goyat, V., Verma, S., & Garg, R. K. (2017). Reduction of stress concentration for a rounded rectangular hole by using a functionally graded material layer. *Acta Mechanica, 228*(10), 3695-3707.

Goyat, V., Verma, S., & Garg, R. K. (2018). On the reduction of stress concentration factor in an infinite panel using different

radial functionally graded materials. *International Journal of Materials and Product Technology, 57*(1-3), 109-131.
Goyat, V., Verma, S., & Garg, R. K. (2018). Reduction in stress concentration around a pair of circular holes with functionally graded material layer. *Acta Mechanica, 229*(3), 1045-1060.
Griffith, A. A. (1921). VI. The phenomena of rupture and flow in solids. *Philosophical transactions of the royal society of london. Series A, containing papers of a mathematical or physical character, 221*(582-593), 163-198.
Gross, B. (1964). Stress-intensity factors for a single-edge-notch tension specimen by boundary collocation of a stress function. *National Aeronautics and Space Administration*.
Gu, P., & Asaro, R. J. (1997). Crack deflection in functionally graded materials. *International Journal of Solids and Structures, 34*(24), 3085-3098.
Gu, P., Dao, M., & Asaro, R. J. (1999). A simplified method for calculating the crack-tip field of functionally graded materials using the domain integral.
Ham, S., & Hong, H. (2018). XFEM fracture analysis by applying smoothed weighted functions with compact support. *Engineering Solid Mechanics, 6*(3), 227-240.
Heidari-Rarani, M., & Sayedain, M. (2019). Finite element modeling strategies for 2D and 3D delamination propagation in composite DCB specimens using VCCT, CZM and XFEM approaches. *Theoretical and Applied Fracture Mechanics, 103*, 102246.
Hosseini, S. S., Bayesteh, H., & Mohammadi, S. (2013). Thermo-mechanical XFEM crack propagation analysis of functionally graded materials. *Materials science and engineering: A, 561*, 285-302.
Inglis, C. E. (1913). Stresses in a plate due to the presence of cracks and sharp corners. *Trans Inst Naval Archit, 55*, 219-241.
Irwin, G. R. (1957). Analysis of stresses and strains near the end of a crack traversing a plate.
Kim, J. H., & Paulino, G. H. (2002). Isoparametric graded finite elements for nonhomogeneous isotropic and orthotropic materials. *Journal of Applied Mechanics, 69*(4), 502-514.
Kim, J. H., & Paulino, G. H. (2005). Consistent formulations of the interaction integral method for fracture of functionally graded materials.
Koizumi, M., & Niino, M. (1995). Overview of FGM research in Japan. *Mrs Bulletin, 20*(1), 19-21.
Kubair, D. V., & Bhanu-Chandar, B. (2008). Stress concentration factor due to a circular hole in functionally graded panels under uniaxial tension. *International Journal of Mechanical Sciences, 50*(4), 732-742.
Mirmohammad, S. H., Safarabadi, M., Karimpour, M., Aliha, M. R. M., & Berto, F. (2018). Study of composite fiber reinforcement of cracked thin-walled pressure vessels utilizing multi-scaling technique based on extended finite element method. *Strength of Materials, 50*(6), 925-936.
Moës, N., Dolbow, J., & Belytschko, T. (1999). A finite element method for crack growth without remeshing. *International journal for numerical methods in engineering, 46*(1), 131-150.
Mohammadi, M., Dryden, J. R., & Jiang, L. (2011). Stress concentration around a hole in a radially inhomogeneous plate. *International Journal of Solids and Structures, 48*(3-4), 483-491.
Paulino, G. H., & Kim, J. H. (2004). A new approach to compute T-stress in functionally graded materials by means of the interaction integral method. *Engineering Fracture Mechanics, 71*(13-14), 1907-1950.
Rao, B. N., & Rahman, S. (2003). An interaction integral method for analysis of cracks in orthotropic functionally graded materials. *Computational mechanics, 32*(1), 40-51.
Sburlati, R. (2013). Stress concentration factor due to a functionally graded ring around a hole in an isotropic plate. *International Journal of Solids and Structures, 50*(22-23), 3649-3658.
Sburlati, R., Atashipour, S. R., & Atashipour, S. A. (2014). Reduction of the stress concentration factor in a homogeneous panel with hole by using a functionally graded layer. *Composites Part B: Engineering, 61*, 99-109.
Shi, P. P. (2015). Stress field of a radially functionally graded panel with a circular elastic inclusion under static anti-plane shear loading. *Journal of Mechanical Science and Technology, 29*(3), 1163-1173.
Singh, I. V., Mishra, B. K., & Bhattacharya, S. (2011). XFEM simulation of cracks, holes and inclusions in functionally graded materials. *International Journal of Mechanics and Materials in Design, 7*(3), 199-218.
Yang, Q., & Gao, C. F. (2016). Reduction of the stress concentration around an elliptic hole by using a functionally graded layer. *Acta Mechanica, 227*(9), 2427-2437.
Yang, Q., Gao, C. F., & Chen, W. (2010). Stress analysis of a functional graded material plate with a circular hole. *Archive of Applied Mechanics, 80*(8), 895-907.
Yang, Q., Gao, C., & Chen, W. (2012). Stress concentration in a finite functionally graded material plate. *Science China Physics, Mechanics and Astronomy, 55*(7), 1263-1271.
Yang, Q., Zhu, W., Li, Y., & Zhang, H. (2018). Stress field of a functionally graded coated inclusion of arbitrary shape. *Acta Mechanica, 229*(4), 1687-1701.
Zeleke, M., Dintwa, E., & Nwaigwe, K. (2021). Stress intensity factor computation of inclined cracked tension plate using XFEM. *Engineering Solid Mechanics, 9*(4), 363-376.